

# HAFIT: Human-Centered AI for Fashion Image Translation

Jianan Jiang  
Hunan University  
Changsha, Hunan, China  
jiangjn22@hnu.edu.cn

Xinglin Li  
Hunan University  
Changsha, Hunan, China  
lixinglin@hnu.edu.cn

Weiren Yu  
University of Warwick  
Coventry, CV4 7AL, UK  
Weiren.Yu@warwick.ac.uk

Di Wu  
Hunan University  
Changsha, Hunan, China  
dwu@hnu.edu.cn

**Abstract**—In the realm of fashion design, sketches serve as the canvas for expressing an artist’s distinctive drawing style and creative vision, capturing intricate details like stroke variations and texture nuances. The advent of sketch-to-image cross-modal translation technology has notably aided designers. However, existing methods often compromise these sketch details during image generation, resulting in images that deviate from the designer’s intended concept. This limitation hampers the ability to offer designers a precise preview of the final output. To overcome this challenge, we introduce HAFIT, a novel approach that transforms sketches into high-fidelity, lifelike clothing images by integrating multi-scale features and capturing extensive feature map dependencies from diverse perspectives. Through extensive qualitative and quantitative evaluations conducted on our self-collected dataset, our method demonstrates superior performance compared to existing methods in generating photorealistic clothing images. Our method excels in preserving the distinctive style and intricate details essential for fashion design applications. In addition, our method also has obvious advantages in model training and inference speed, contributing to reducing designers’ time costs and improving design efficiency. Code is available at <https://github.com/ExponentiAI/HAFIT/>.

**Index Terms**—Sketch-to-Image Generation; Image-to-Image Translation; Generative Adversarial Networks

## I. INTRODUCTION

In the creative journey of design, sketches serve as the foundational tool for conceptualizing and outlining new pieces, demonstrating the unique styles of different designers. Designers initiate their process by crafting sketches that capture the basic structure of their envisioned creation. Subsequently, through iterative refinement, these sketches evolve, receiving modifications and intricate detailing to further refine the designs. Progressing from these refined stages, designers infuse life into their sketches by adding colors, aiming to impart depth and realism to their representations. Throughout this process, a robust sketch-to-image method plays a crucial role. It not only allows designers to preview renderings of colored sketches, aiding in refining the sketchwork, but also facilitates the generation of diverse image styles to inspire their designs.

In the earlier research, methods like Sketch2Photo [4] synthesized realistic images by amalgamating object and background images derived from provided sketches. They laid the groundwork for deep learning techniques. The emergence of Generative Adversarial Networks (GAN) [7] marked a significant shift in this domain, with methods such as BicycleGAN [40], pix2pix [14], and others [13], [18], [21], [35]



Fig. 1. The performance of different methodological approaches [20], [33] compared to ours in handling sketch details (zooming in for better visual).

gaining prominence. Although these methods have showcased notable results, preserving sketch details remains a challenge, as illustrated in Fig. 1. Through our comparison of two classic algorithms based on GAN [33] and Diffusion Model (DM) [20], we discovered significant hurdles in retaining sketch details. Specific elements such as clothing necklines, pockets, sleeves, and other intricate details prove challenging to effectively express in the lines of the designer’s sketches. This limitation significantly hampers designers’ ability to preview and enhance finer details and refinements within sketches.

In recent years, with the introduction of the diffusion model [10], a novel and improved image generation algorithm has swiftly emerged. Some works, such as DDIM [30], employ skip sampling to expedite the model’s inference process, while LDM [26] utilizes feature mapping to execute the diffusion process in the latent space, effectively mitigating the issue of high resource requirements for model training. Additionally, Palette [28] and BBDM [20] showcase the efficacy of diffusion models in image translation tasks. However, these methods heavily rely on extensive data for learning and demand substantial computing resources. Consequently, they still face significant challenges in model training, inference, and fine-tuning, resulting in high time and resource costs, which may not be user-friendly for designers.

To address these challenges, we introduce HAIFIT (**H**uman-Centered **AI** for **F**ashion **I**mage **T**ranslation), a GAN-based creative generation network designed for sketch-to-image translation in fashion design. HAIFIT aims to empower designers to foster inspiration by preserving as much detail as possible from their sketches in the generated images. Specifically, HAIFIT focuses on converting clothing sketches into high-quality realistic clothing images using a pyramidal generative adversarial network. To facilitate this conversion, we have developed a customized *Multi-scale Feature Fusion Encoder* (MFFE) that maps the reference hand-drawn sketches and generated images into a shared latent space. MFFE comprises a *Shallow Convolution Module* (SCM) and an *Abstract Feature Representation Module* (AFRM), which enables the capture of long-term dependencies between different regions and improves the global correlation in feature representations. Furthermore, we enhance the fine-grained features among generated images of various scales by integrating the Cross-level Skip Connection Module (CSCM) within the feature space across different layers. By employing multi-scale discriminators, we ensure the preservation of global structural integrity while emphasizing fine details, resulting in more realistic generated images.

The key **contributions** of our work are summarised as follows:

- **Methodology.** To the best of our knowledge, we are the pioneers in treating sketch features as sequence inputs, ensuring consistency by inputting features from both forward and reverse feature sequences. This innovative approach enhances the representation of details in the generated images. Moreover, we are the first to propose a Pyramid Diffusion Model, which uses a progressive generation approach to improve the quality of model generation.
- **Structure.** We introduce the LSTM-based MFFE to enhance the representation of global features and ensure coherence and consistency in the latent space. Additionally, our CSCM strategically directs the model’s attention to finer sketch details, contributing to improved and more nuanced sketch feature representation.
- **Datasets.** We construct a background-free dataset comprising fashion clothes and their corresponding sketches for cross-modal image translation tasks, filling the gap in this field.
- **Performance.** Our method demonstrates superior performance in extensive quantitative and qualitative experiments compared to various baselines.

The rest of the article is structured as follows: Sec. II provides an overview of the work and technological progress related to image translation. Sec. III presents the technical details of our approach. Sec. IV introduces a version of our method extended to a diffusion model. Sec. V presents the experimental results of our approach. Sec. VI summarizes our work.

## II. RELATED WORK

### A. Sketch-to-Image Generation

The task of sketch-to-image generation falls within the realm of image translation, a pivotal objective in computer graphics and computer-human interaction. In the domain of fashion clothing design, having an effective algorithm that can accurately generate diverse clothing images based on designers’ sketches is invaluable. Such algorithms enable designers to express their creative ideas effectively, save development time, and enhance design efficiency. Early methods, like Photosketcher [6], utilized local features for image retrieval and employed graphics techniques to segment and stitch images together to achieve sketch-to-image generation. Subsequently, with the development of convolutional neural networks [8], [19], [29], [31], deep learning-based methods have become the mainstream approach for achieving sketch-to-image generation. Isola et al. [14] introduced a unified framework for image-to-image translation models adaptable to various scenarios. This framework facilitates mapping segmented images to natural images or converting edge maps to color images, among other applications. Building upon this, Pix2piHD [33] utilized multi-scale generators and discriminators to achieve high-resolution image translation. Several other methods [1], [13], [18], [21] have improved image generation performance by incorporating attention networks, innovative adversarial loss functions, or different image features. However, these methods still encounter challenges in handling complex strokes and refining synthetic structures to produce realistic images. In summary, synthesizing an image that faithfully represents the content of a sketch while maintaining consistent styles is paramount.

### B. Generative Adversarial Networks

The Generative Adversarial Network (GAN) comprises two components: the generator and the discriminator. It leverages adversarial training to enhance the generator’s ability to generate realistic images, yielding significant achievements in image generation, restoration, and various other domains. Initially proposed by Goodfellow et al. [7]. For generating realistic data, GANs have since undergone several extensions and improvements. Mirza et al. [23] extended the GAN to enable the generation of images with specific conditions, allowing users to control attributes such as image categories. Radford et al. [25] introduced convolutional neural networks into both the generator and discriminator, thereby enhancing GAN’s ability to capture spatial image features. Zhu et al. [39] achieved cross-domain image conversion by introducing a cycle consistency loss function, enabling realistic transformations from one domain to another, such as from horse to zebra. Karras et al. [17] achieved stable control over the style and diversity of generated images by introducing style variables. Brock et al. [3] further scaled up the GAN and improved training methods to generate high-resolution images. Additionally, methods like WGAN [2], PGGAN [16], and SAGAN [37] have introduced new optimization losses,

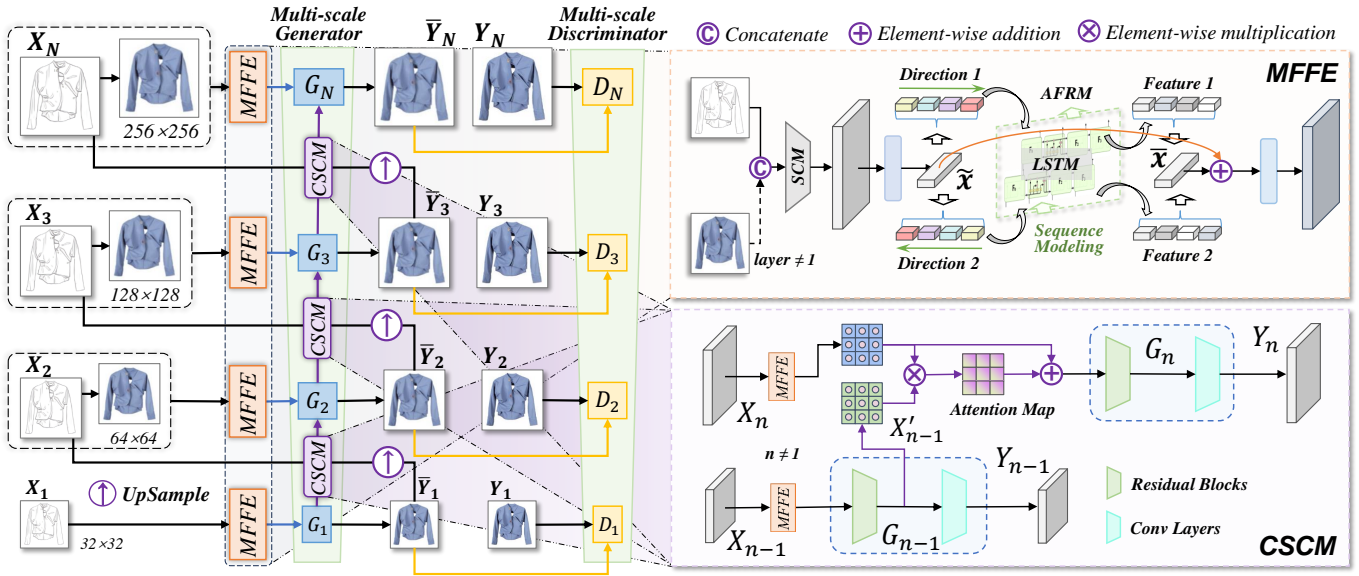


Fig. 2. (i) [Left] The illustration of our HAIFIT architecture. Given  $M$  paired sketch-image samples  $\{(x_i, y_i) \in (X, Y)\}_{i=1}^M$ , our goal is to map images from hand-drawn sketches domain  $X$  to realistic images domain  $Y$ , while preserving as many line details from the sketch  $X$  as possible in the generated image  $\bar{Y}$ . (ii) [Top Right] An overview of the Multi-scale Feature Fusion Encoder (MFFE). (iii) [Bottom Right] An overview of the Cross-level Skip Connection Module (CSCM).

multi-layer resolution training strategies, and self-attention mechanisms to achieve more stable GAN training and further enhance the quality and diversity of generated images. In general, the continuous development and evolution of GANs have unlocked significant potential in the field of image generation, transforming the generation of realistic images from a concept into reality. Compared to the recent diffusion models [20], [28], GANs possess the advantages of low hardware costs and fast synthesis speed, thus continuing to play a key role in the design field.

### C. Diffusion Models

Different from GANs, the diffusion model [10] realizes image generation from a novel perspective. It comprises two stages: the forward noise-adding stage and the reverse denoising stage. In the forward noise-adding stage, Gaussian noise is continuously added to the initial input data to make it approximately Gaussian. In the reverse denoising stage, the model is tasked with recovering the original input data by learning to gradually reverse the denoising process. Diffusion models are widely appreciated for the quality and diversity of the samples they generate, but they also impose a severe computational burden and time cost. DDIM [30] addresses the issue of single-step sampling in the inference process through skip sampling. Subsequent advancements like ADM [5] further demonstrate the superiority of the diffusion model over traditional GAN methods in image synthesis. Another notable approach by Ho et al. [11] proposes a diffusion model training method without classifier guidance. Palette [28] introduces a unified framework for image-to-image translation based on the conditional diffusion model, achieving superior results across multiple image generation subtasks. However, they still

encounter significant model training costs. LDM [26] addresses this by significantly reducing model training costs and opening up new avenues for subsequent research by placing the diffusion process in latent space. DiT [24] explores a new class of diffusion models based on transformer architecture, enhancing the scalability and quality of diffusion models. Overall, these studies continuously advance the field of image generation and offer new possibilities for natural and realistic image synthesis.

## III. METHODOLOGY

In this study, we present HAIFIT, as depicted in Fig. 2, which draws on the training strategy of PGGAN [16] and comprises two core components: the *Multi-scale Feature Fusion Encoder* (MFFE), and the *Cross-level Skip Connection Module* (CSCM). The MFFE is used to get global contour features and abstract intent features. Then the feature maps are resized and concatenated at multiple scales before being fed into the multi-scale pyramid generator, which can produce realistic images with complete structures and exquisite details.

### A. Multi-scale Feature Fusion Encoder

The *Multi-scale Feature Fusion Encoder* (MFFE) consists of two modules: the *Shallow Convolutional Module* (SCM) and the *Abstract Feature Representation Module* (AFRM). As illustrated in Fig. 2 (ii), the SCM employs a convolutional network to learn essential global contour information, such as the structure of the object. Simultaneously, inspired by the LSTM architecture [12], we design the AFRM to learn long-range dependencies in key areas of the input sketch from various perspectives, which can effectively capture style features and geometric features of strokes. By combining

these features, we can effectively capture the consistency of objects' complete structure and intricate textures within the latent space.

As shown in Fig. 2 (i), in the bottom layer, only the sketch features are inputted. In the other layers, we perform element-wise addition between the generated image features and the sketch features, and then input the resulting summed features into the MFFE. In the SCM we employ a sequence of convolutional layers, denoted as *Con*, to extract the global contour features and shape information  $\tilde{x}$  from the input sketch  $x_s$ . Here,  $x_s \in \mathcal{R}^{b \times 3 \times m \times m}$ ,  $\tilde{x} \in \mathcal{R}^{b \times 256 \times m/4 \times m/4}$ ,  $b$  is the batch size, and  $m$  depends on the network layer, so we can express this process as  $\tilde{x} = Con(x_s)$ . Specifically, the SCM extracts features in a blockwise manner, which will disrupt the continuity of strokes and result in pixel-level contour features. Since sketches are continuous and composed of multiple lines in different directions, it is crucial to consider the correlation between adjacent lines in order to effectively learn the line features of complex sketches.

To address this issue, we introduce the AFRM to learn the feature  $\tilde{x}$ . The AFRM consists of a two-layer LSTM network, capturing abstract drawing intent features from four directions. After downsampling  $\tilde{x}$ , we obtain the feature  $\tilde{x}' \in \mathcal{R}^{b \times 256 \times 4 \times 4}$ . We then swap feature positions after merging its second and third dimension features to obtain  $\mathcal{R}^{4 \times b \times 1 \times 1024}$  and divide it into four parts, namely  $\tilde{x}_0, \tilde{x}_1, \tilde{x}_2$ , and  $\tilde{x}_3$ , with dimensions  $\mathcal{R}^{b \times 1 \times 1024}$ . These features are then individually sequence inputted into the LSTM network, generating features  $\bar{x}_0, \bar{x}_1, \bar{x}_2$ , and  $\bar{x}_3$  by recursively processing the input features from different directions. Next, we concatenate the features  $\bar{x}_0, \bar{x}_1, \bar{x}_2$ , and  $\bar{x}_3$  to obtain the feature  $\bar{x}' \in \mathcal{R}^{4 \times b \times 1 \times 1024}$ . Afterward, we restore the dimension of  $\bar{x}'$  to the dimension of  $\tilde{x}'$ . Finally, we apply a  $1 \times 1$  convolutional layer along the channel dimension to obtain the output feature  $\bar{x} \in \mathcal{R}^{b \times 256 \times 4 \times 4}$ .

The MFFE is employed to learn features from different perspectives of the sketches, which enables us to capture variations in lines and abstract painting intentions in crucial areas of the sketches. In the task of sketch-to-image generation, it is vital for the encoder to acquire diverse line patterns and painterly intent in clothing patterns and details. Failure to do so can severely impact the visual quality of the synthesized image, even if the overall generation quality is satisfactory. As a result, to further ensure the consistency of the generated images, we introduce the concept of reverse sketch feature input. This is because a sketch should yield consistent results regardless of the direction it is interpreted from. As shown in Fig. 2, we provide the structural details related to the AFRM in MFFE. We serialize the feature  $\tilde{x}$  obtained from the SCM and input it into the AFRM through forward and reverse feature inputs. The output features  $\bar{x}'_{for}$  and  $\bar{x}'_{rev}$  are then fused to obtain the unified sketch abstract stroke feature  $\bar{x}$ , which is subsequently used in the later stages of the model. Therefore,

the aforementioned process can be summarized as follows:

$$\begin{aligned}\bar{x}'_{for} &= Cat(LSTM[\tilde{x}_0, \tilde{x}_1, \tilde{x}_2, \tilde{x}_3]) \\ \bar{x}'_{rev} &= Cat(LSTM[\tilde{x}_3, \tilde{x}_2, \tilde{x}_1, \tilde{x}_0]) \\ \bar{x} &= Conv_{1 \times 1}(Cat(\bar{x}'_{for}, \bar{x}'_{rev}))\end{aligned}\quad (1)$$

Finally, we fuse the global structure feature  $\tilde{x}$  and abstract intention feature  $\bar{x}$  through a differentiable parameter  $\zeta$  with the initial value of 1.0 to get the embedded sketch feature  $x$ :

$$x = \zeta \tilde{x} + \bar{x} \quad (2)$$

### B. Cross-level Skip Connection Module

In order to effectively capture intricate details in the key areas of the sketch, we employ a pyramid generative learning approach [16] with a *Cross-level Skip Connection Module* (CSCM). Our model comprises a pyramid of generators  $G_n \in \{G_1, G_2, \dots, G_N\}$ , which are trained using a set of multi-scale images  $x_i$  represented as  $x_i^1, x_i^2, \dots, x_i^N$ . Each generator  $G_n$  is responsible for generating a realistic image  $\bar{y}_i^n$ . By adversarial training, the generator  $G_n$  aims to deceive the associated discriminator  $D_n \in \{D_1, D_2, \dots, D_N\}$ , and the  $D_n$  is trained to distinguish between the generated realistic images and real images. The generation of a realistic image sample starts at the coarsest scale  $64 \times 64$  and sequentially passes through all generators, progressing toward the finest scale  $256 \times 256$ . At the coarsest scale, the MFFE takes a minibatch of the sketch feature maps  $X_n$  as input. The effective receptive field at this level is typically half the height of the finer image. Each of the generators  $G_n$  at finer scales adds details that are not generated by the previous scales. Therefore, in addition to the feature maps  $X_n$ , each multi-scale feature fusion encoder accepts an upsampled version of the generated image features from the coarser scale. Here,  $X_n \in \mathcal{R}^{b \times 3 \times m \times m}$ ,  $Y_{n-1} \in \mathcal{R}^{b \times 3 \times m/2 \times m/2}$ . This pyramid structure allows us to capture features at multiple scales and better handle the complex details of the sketch.

$$Y_n = \begin{cases} G_n(X_n), & \text{if } n = 1 \\ G_n(X_n, Y_{n-1}), & \text{if } n > 1 \end{cases} \quad (3)$$

The generator  $G_n$  consists of a residual block and multiple convolutional layers. In the coarsest layer, the residual block comprises four convolutional layers. In addition, in the pyramid network, as the number of pixels increases from bottom to top, the residual block progressively adds one convolutional layer at each level. This progressive increment facilitates the learning of sketch feature representations. Through numerous experiments, it has been observed that incorporating the CSCM between different layers in the pyramid network can enhance the quality of the generated images, which is illustrated in Fig. 2 (iii). In detail, We extract the output feature  $X'_{n-1}$  from the last layer of the residual block in generator  $G_{n-1}$  and concatenate it with the output feature  $X_n$  from the  $n$ -th layer of the MFFE. Subsequently, we use  $\bar{X}_n$  as the input for generator  $G_n$ , where  $\bar{X}_n \in \mathcal{R}^{b \times 256 \times m \times m}$ . In principle, the multi-level features of the same synthetic image should exhibit similarity. By employing cross-level feature operations, we can

---

**Algorithm 1** The Diffusion HAIFIT Training Process.

**Require:**  $S$ : Input Sketches  
**Require:**  $E$ : Sketch Encoder network  
**Require:**  $\epsilon$ : Gaussian Noise  
**Require:**  $step$ : Model training steps  
**Require:**  $t \in [0, 1000]$ : Diffusion moment  
**Require:**  $G_i \in \{G_1, G_2, G_3, G_4\}$ : Generator networks  
**Require:**  $\bar{Y}_i \in \{\bar{Y}_1, \bar{Y}_2, \bar{Y}_3, \bar{Y}_4\}$ : Generated Images  
1: Randomly initialize  $\epsilon$  as Input  
2: **for**  $i = 1$  to 4 **do**  
3:     Utilize  $E$  to encode  $S$  as supervised conditions  
4:     **for** 0 to  $step$  **do**  
5:         Randomly initialize  $t$   
6:         Train  $G_i$  to predict the  $t$ -th moment noise  $\bar{\epsilon}_t$   
7:         Compute loss between  $\bar{\epsilon}_t$  and real noise  $\epsilon_t$   
8:         Update parameters of  $G_i$  using gradient descent  
9:     **end for**  
10:    **if**  $i < 4$  **then**  
11:        Freeze parameters in  $G_i$  and use it for inference  
12:        Upsample  $\bar{Y}_i$  to double its original resolution and concatenate with new resolution  $\epsilon$  as Input  
13:     **end if**  
14: **end for**  
15: Utilize all  $\{G_i\}_{i=1}^4$  for inference generation

---

extract similar details from the features generated by different level generators and incorporate them as attention maps into the new feature map  $X_n$ . This facilitates image translation, resulting in more detailed and high-quality images.

$$\begin{aligned} \bar{X}_n &= X_n + X_n \cdot X'_{n-1} \\ Y_n &= G_n(\bar{X}_n, Y_{n-1}), n = 2, 3, 4 \end{aligned} \quad (4)$$

### C. Loss Function

Our full loss function consists of L1 loss, adversarial loss, style loss, and perceptual loss. We empirically set the following parameters:  $\lambda_{l1}=1.5$ ,  $\lambda_{adv}=10.0$ ,  $\lambda_{per}=0.1$ ,  $\lambda_{style}=250.0$ , to keep stable training and higher-quality results.

$$\mathcal{L}_S = \lambda_{l1}\mathcal{L}_{l1} + \lambda_{adv}\mathcal{L}_{adv} + \lambda_{style}\mathcal{L}_{style} + \lambda_{per}\mathcal{L}_{per} \quad (5)$$

**L1 Loss.** We directly employ the L1-distance loss to enhance the similarity between the pixel features of the generated image  $G(x)$  and the real image  $y$ .

$$\mathcal{L}_{l1} = \|y - G(x)\|_1 \quad (6)$$

**Adversarial Loss.** To improve the quality of generated samples, we utilize the vanilla GAN [7] min-max loss for the generator  $G$  and discriminator  $D$  training process.

$$\mathcal{L}_{adv} = \mathbb{E}_y[\log D_Y(y)] + \mathbb{E}_x[\log(1 - D_Y(G(x)))] \quad (7)$$

**Style Loss.** We incorporate the *Gram* matrices-based loss to better reproduce the texture details of input sketches  $x$ .

$$\mathcal{L}_{style} = \|Gram(y) - Gram(G(x))\|_1 \quad (8)$$

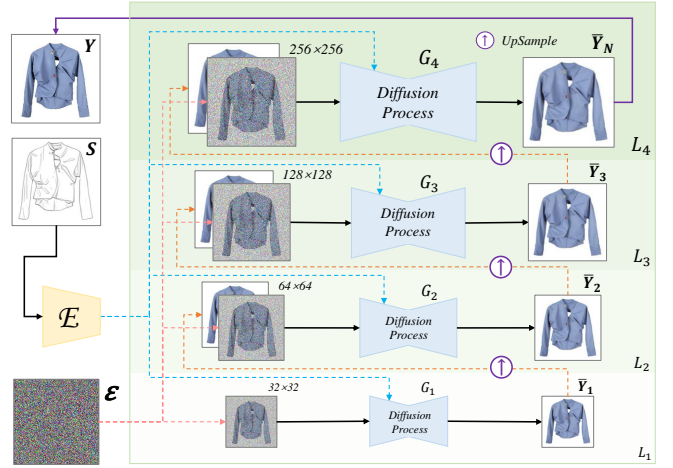


Fig. 3. The illustration of our HAIFIT with Diffusion model architecture.

**Perceptual Loss.** To ensure both semantic similarity between the generated image and its ground truth, as well as encourage the network to generate diverse images, we employ the pre-trained VGG-16 [29]  $\phi$  to extract  $L$ -levels features.

$$\mathcal{L}_{per} = \sum_{i=1}^{L=5} \frac{1}{N_i} \|\phi_i(y) - \phi_i(G(x))\|_1 \quad (9)$$

## IV. PYRAMID DIFFUSION MODEL

In recent years, the Diffusion models [10], [26], [30] have garnered significant attention from researchers due to their potent generation capabilities, leading to rapid advancements and widespread adoption across various fields. Building upon this, we extend our GAN-based HAIFIT model to incorporate a diffusion model version: the Pyramid Diffusion Model.

### A. Preliminaries of DDPM

The Denoising Diffusion Probabilistic Model (DDPM) comprises a forward process and a reverse process. In the forward process, noise  $\epsilon$  is iteratively added to the original image  $X_0$ , resulting in a noisy image  $X_T$ . The noise  $\epsilon$  added at each time step  $t$  is sampled from a Gaussian distribution  $\mathcal{N}(0, I)$ . When  $T$  is sufficiently large, we believe that  $X_T$  approximately conforms to the Gaussian distribution, here we set  $T = 1000$ . This transmission can be mathematically represented as  $q(X_t|X_{t-1}) = \mathcal{N}(\sqrt{1-\beta_t}X_{t-1}, \beta_t I)$ ,  $\{\beta_t\}_{t=0}^T \in (0, 1)$ . Therefore, the noised image  $X_t$  at  $t$ -th moment in the forward process can be expressed as:

$$X_t = \sqrt{\bar{\alpha}_t}X_0 + \sqrt{(1-\bar{\alpha}_t)}\epsilon, \epsilon \sim \mathcal{N}(0, I) \quad (10)$$

where  $\alpha_t = 1 - \beta_t$  and  $\bar{\alpha}_t = \prod_{i=1}^t \alpha_i$ .

In the reverse process stage, the noisy image  $X_T$  is continuously denoised to revert it back to the original input image  $X_0$ . This is achieved by training a model  $\theta$  to predict the noise  $\epsilon$  added to at each time step  $t$ , thereby removing the corresponding noise  $\epsilon$ . Therefore, the approximate probability distribution of the image  $X_{t-1}$  at time  $t$  can be expressed as:

$$p_\theta(X_{t-1}|X_t) = \mathcal{N}(X_{t-1}; \mu_\theta(X_t, t), \sigma^2 I) \quad (11)$$

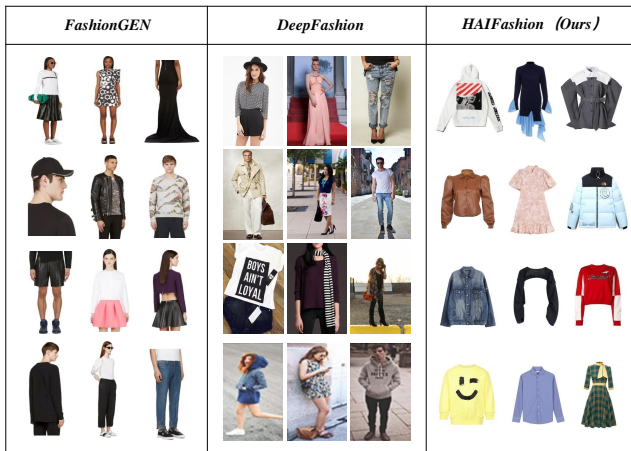


Fig. 4. Existing fashion datasets FashionGEN [27] and DeepFashion [22] compared to our newly proposed dataset, HAIFashion.

To summarize, the optimization objective function of the diffusion model training process is:

$$\mathcal{L}(\theta) = \mathbb{E}_{x, \epsilon \sim \mathcal{N}(0,1), t} \left[ \|\epsilon - \epsilon_\theta(x_t, t)\|_2^2 \right] \quad (12)$$

### B. Diffusion HAIFIT

As presented in Fig. 3, We utilize the diffusion method to hierarchically train each layer in HAIFIT. Beginning from the  $L_1$  layer, we progressively train upwards to the  $L_4$  layer. Upon completing the training of the previous layer network, we freeze the parameters of the network and add a new layer network upwards for further training until all layers of the model are trained. Specifically, we initialize random noise  $\epsilon$  and then train  $G_1$  to predict the noise  $\epsilon_t$  at each moment  $t$  and perform denoising operations on  $X_t$  until  $G_1$  effectively simulates the noise value added at each moment  $t$ , where  $t \in [0, 1000]$ . During this process, we employ an encoder  $E$  to encode the features of the corresponding sketch  $S$  for supervised diffusion model training. This encoder is a backbone based on a pre-trained ResNet [8]. We adjust the dimension of the final encoded feature output by adding a trainable linear layer behind the backbone. Once  $G_1$  training is complete, we freeze the parameters in  $G_1$  and utilize it for inference, subsequently training the parameters in  $G_2$ . The input of  $G_2$  contains both the noised image  $X_t$  at the resolution of this layer and the low-resolution image  $\bar{Y}_1$  generated by  $G_1$ . We upsample  $\bar{Y}_1$  to double its original resolution and then concatenate it with the noised image  $X_t$  in the channel dimension before inputting it into  $G_2$ . Following a similar procedure, we train the generators  $G_3$  and  $G_4$  successively. Upon completion of training, we utilize all layers in the model for inference generation. The principle of our Diffusion version of HAIFIT can be referenced in Algorithm 1.

## V. EXPERIMENTS

### A. HAIFashion Dataset

Considering our objective of learning clothing sketch features and generating high-quality clothing images while pre-

serving the designer’s style and intricate details, it’s imperative to construct a new clothing dataset comprising paired images and sketches for model training and testing. While directly hand-drawing a large dataset of garment image-sketch pairs by designers may seem challenging, a more feasible approach involves designers creating a small amount of clothing image-sketch paired data, which can then be expanded using an image-to-sketch generation algorithm. Thanks to the personalized sketch generation algorithm proposed by StyleMe [35], this dataset construction becomes feasible. Thus, our dataset construction task focuses on building a fashion clothing image dataset for image-to-sketch generation.

Common publicly available fashion datasets like FashionGEN [27] and DeepFashion [22] predominantly feature realistic fashion images sourced directly from real-world photos. These images often include various backgrounds and individuals wearing the clothing in social settings. However, images with backgrounds pose significant challenges in generating single clothing sketches, which may not meet our requirements. The comparison between these datasets is illustrated in Fig. 4. In this study, we introduce a self-collected clothing dataset named HAIFashion. HAIFashion comprises 3100 pairs of fashion clothing image-sketch datasets. We achieved this by crawling 3100 background-free fashion clothing images from the internet and employing the sketch generate algorithm [35] and the paired sketch-image dataset [15] to generate designer-style clothing sketches, facilitating our experiments.

### B. Implementation Details

We implement our model on Pytorch and all experiments are performed on a single NVIDIA GeForce RTX4090 GPU. We utilize the Adam optimizer with a learning rate of 1e-4 for the generator and 5e-4 for the discriminator, the batch size is set to 8. The learning rates decayed at the halfway point every 100 epochs. The training process continued until the SSIM [34] showed no improvement for 10 iterations. For the dataset, we use our proposed HAIFashion (§ V-A) and divide it into 2500 (600) for model training and testing respectively.

### C. Evaluation Metrics

We employ four commonly used quantitative evaluation metrics:

- **PSNR** (Peak Signal-to-Noise Ratio) assesses image quality by comparing the peak signal-to-noise ratio between the original image and the generated image. Higher PSNR values indicate smaller differences between the images and higher-quality generated images.
- **SSIM** (Structural Similarity Index) [34] evaluates image quality by comparing the structural similarity between the original image and the generated image. It considers similarities in brightness, contrast, and structure to calculate the final score. Larger SSIM values signify higher similarity between the images and better generation effects.
- **LPIPS** (Learned Perceptual Image Patch Similarity) [38] assesses image quality by utilizing a deep learning model and the L2 norm to calculate the perceptual difference

TABLE I  
THE OVERALL SKETCH-TO-IMAGE GENERATION PERFORMANCE ON THE HAIFASHION DATASET. (↑ INDICATES THE HIGHER VALUE, THE BETTER EFFECT. ↓ INDICATES THE LOWER VALUE, THE BETTER EFFECT.)

Methods	Venue	Architecture	Structural			Perceptual		
			PSNR ↑	SSIM ↑	Overall ↑	LPIPS ↓	FID ↓	Overall ↓
BicycleGAN [40]	NeurIPS'17	GAN-based	12.3482	0.4258	12.7740	0.1976	70.6381	70.8357
pix2pix [14]	CVPR'17	GAN-based	<b>19.2761</b>	0.3826	<u>19.6587</u>	0.1180	48.3830	48.5010
MUNIT [13]	ECCV'18	GAN-based	13.3265	0.4843	13.8108	0.1947	74.2733	74.4680
UAGITI [1]	NeurIPS'18	GAN-based	11.8259	0.0901	11.9160	0.2383	83.8309	84.0692
pix2pixHD [33]	CVPR'18	GAN-based	16.1863	<u>0.5622</u>	16.7485	<u>0.1026</u>	<u>48.0041</u>	<u>48.1067</u>
USTP [21]	ECCV'20	GAN-based	13.2456	<u>0.5126</u>	13.7582	0.1429	58.8756	59.0185
UGATIT [18]	ICLR'20	GAN-based	12.8841	0.4799	13.3640	0.1783	83.9190	84.0973
IrwGAN [36]	ICCV'21	GAN-based	17.2878	0.4555	17.7433	0.1061	71.7609	71.8670
Palette [28]	SIGGRAPH'22	DM-based	7.8216	0.0787	7.9003	0.3591	116.9303	117.2894
BBDM [20]	CVPR'23	DM-based	14.9788	0.5343	15.5131	0.1676	59.7919	59.9595
<b>HAIFIT</b>	Ours	GAN-based	<u>19.0660</u>	<b>0.6338</b>	<b>19.6998</b>	<b>0.0778</b>	<b>28.5032</b>	<b>28.5810</b>

between the generated image and the original image in the feature space. Lower LPIPS values suggest better-quality images.

- **FID** (Fréchet Inception Distance) [9] evaluates image quality by comparing the statistical distribution in the feature space of the generated image with that of the original image. It employs the Fréchet distance to measure the similarity between the distributions. Lower FID values indicate higher-quality resulting images.

The first two metrics primarily gauge the completeness and structural similarity of the generated images, whereas the latter two metrics focus more on assessing the diversity, authenticity, and perceptual differences of the generated images.

#### D. Baselines

In our experiments, we compared our method with ten state-of-the-art baseline approaches. All models undergo identical preprocessing steps and are trained directly following the official open-source code to ensure a fair comparison.

- **BicycleGAN** [40] focuses on modeling a distribution of possible outputs in a conditional generative model, enhancing the diversity of generated images.
- **pix2pix** [14] implements image translation using conditional GAN to convert input images between different domains.
- **MUNIT** [13] achieves image synthesis by decomposing image representations into content and style properties.
- **UAGITI** [1] incorporates attention networks to minimize divergence between relevant parts of the data-generating distribution.
- **pix2pixHD** [33] utilizes a novel adversarial loss and new multi-scale generator and discriminator architectures in conditional GAN for high-resolution image synthesis.
- **USTP** [21] learns from unpaired sketch and photo data and tackles synthesis through shape translation and content enrichment stages.
- **UGATIT** [18] employs an attention module and a learnable normalization function to enhance the quality and diversity.

- **IrwGAN** [36] introduces the concept of importance-based reweighting to select images and devises a method to learn the weights autonomously while simultaneously conducting image translation.
- **Palette** [28] proposes a unified framework for image-to-image translation based on conditional diffusion models, demonstrating the importance of self-attention.
- **BBDM** [20] presents a novel image-to-image translation approach utilizing the Brownian bridge diffusion model, which enables direct learning of domain translation through a bidirectional diffusion process.

#### E. Comparison Results

**Quantitative Experiments.** We conducted quantitative evaluations to compare both the realism and faithfulness of the generated images. The quantitative results are summarized in Table I, despite achieving the second position in the PSNR index, it is important to note that this result is primarily due to the nature of PSNR, which emphasizes the signal-to-noise ratio and is sensitive to local noise and distortion in the image. HAIFIT, on the other hand, prioritizes retaining more details from the input sketches, including the initial outline, which may lead to a slight decrease in the PSNR index. However, compared to other benchmarks, HAIFIT all achieved first place. In the SSIM metric, our method outperforms the second-placed pix2pixHD model by nearly 13%. For metrics that are more aligned with human visual perception, our method enhances the LPIPS and FID indicators by about 24% and 41% respectively compared to the second-place model, demonstrating superior performance overall. In summary, HAIFIT exhibits excellent performance across all four metrics. This demonstrates the effectiveness of our method in sketch-to-image generation. This success can be attributed to the integration of our proposed MFFE and pyramid generator with CSCM. The MFFE helps our model learn object sketch contours and consider correlations between adjacent lines from different directions, enhancing stroke variation perception. Meanwhile, the pyramid generator with CSCM can capture specific details in key regions of complex sketches, facilitating



Fig. 5. The comparison of sketch-to-image generation from the baselines and our method. The first column is the input sketch, the second column is the corresponding reference image, and the other columns are images generated by different methods.

the learning of the complete structure and fine-tuning of intricate details. The results confirm that our model can well adapt to sketches with specific detailed styles and generate more realistic images.

**Qualitative Experiments.** As shown in Fig. 5, it is evident that our proposed method outperforms other baselines by preserving sketch details and delivering high-definition diverse images. For example, while BicycleGAN, USTP, pix2pixHD, and UGATIT occasionally generate satisfactory results, such as the second row in cycleGAN and USTP, and the third row in pix2pixHD and UGATIT, most of their generated images tend to exhibit a single black tone and lose much of the sketch’s stroke details. Although pix2pix, MUNIT, and IrwGAN methods show better generation effects with good color diversity, they still face numerous challenges. For instance, pix2pix generates colors outside the designated area in the first and sixth rows, and displays abnormal color distribution in the fifth row. MUNIT often loses significant sketch details, causing the edges of the generated images to appear overly smooth and blurry. Moreover, IrwGAN suffers from uneven color distribution in the first, second, and third rows, and a loss of sketch details in the fifth and sixth rows. The UGATIT method consistently shows a red tone in its generated images, along with issues like uneven color distribution, coloring outside the designated areas, and blurred details. In addition, when comparing diffusion models, we find that Palette has serious background coloring issues, making the image background color match the clothing color, and also faces problems with uneven color distribution and loss of sketch details. BBDM, while exhibiting uniform color distribution within contours and avoiding coloring outside the areas, still struggles with

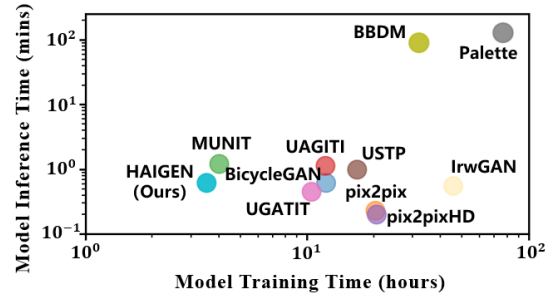


Fig. 6. Comparison of model training and inference times. The coordinate axes adopt a logarithmic value method to better show the positional relationship between them.

retaining fine details in the generated images. Overall, existing methods still struggle with capturing specific complex details in sketches and generating high-definition, diverse images. In contrast, our proposed method excels in handling complex sketches, producing images with more realistic visual effects. **Time Costs.** Fig. 6 illustrates the model training and inference times for our model and the ten baselines. Our model exhibits a clear advantage in training time compared to GAN-based methods. Additionally, when compared to the methods based on the Diffusion model, our model demonstrates an inference time improvement of over 100 times. This significant time-saving advantage can greatly benefit designers by reducing costs, improving work efficiency, and increasing productivity.

#### F. Ablation study

We conduct ablation studies to analyze the effectiveness of (i) the Abstract Feature Representation Module (AFRM) and

TABLE II  
THE QUANTITATIVE EXPERIMENTAL RESULTS ON ABLATION STUDY.

Methods	Structural		Perceptual	
	PSNR $\uparrow$	SSIM $\uparrow$	LPIPS $\downarrow$	FID $\downarrow$
w/o AFRM and CSCM	19.7086	0.6324	0.0812	30.5260
w/o AFRM	19.0474	0.6281	0.0821	31.8295
w/o CSCM	<b>19.7189</b>	0.6294	0.0802	29.9711
Transformer [32]	18.7738	0.6259	0.0814	31.1292
<b>HAI FIT (full)</b>	<u>19.0660</u>	<b>0.6338</b>	<b>0.0778</b>	<b>28.5032</b>



Fig. 7. Qualitative results of the ablation study on HAI FIT.

(ii) the Cross-level Skip Connection Module (CSCM).

**Quantitative Experiments.** As indicated in Table II, the removal of the CSCM between different layers of HAI FIT negatively impacts our model’s performance. CSCM is essential in considering feature correlations across scales and combining different receptive fields, which helps preserve important semantic details. The increase in the PSNR index after removing CSCM is attributed to the loss of sketch detail features, resulting in smoother perceived details. Moreover, removing the AFRM also led to a decline in our model’s performance. AFRM learns long-term dependencies from different perspectives of the sketch using the LSTM module. It takes into account the correlation between adjacent lines in the sketch to increase the details and ensure the consistency of the generated image. Notably, when replacing the LSTM module with the Transformer [32] module, all four performance indicators of the model deteriorated. This decline can be attributed to the temporal dependence offered by the LSTM module, ensuring consistent feature extraction across all directions of the sketch and yielding a more intricate and coherent feature representation. In contrast, the Transformer module, relying on the self-attention mechanism, captures relationships within sequences but lacks strong modeling capabilities in preserving the sequence’s order of features. This outcome underscores the significance of considering the temporal correlation between lines to enhance model performance. Based on the above analysis, the AFRM and CSCM modules enhance our model’s capability to handle complicated sketches. Consequently, HAI FIT enables the generation of high-quality and diverse clothing images while maintaining the complex details of the sketches.

**Qualitative Experiments.** The qualitative results of the ablation study on sketch-to-image generation are presented in Fig. 7. It can be observed that removing the AFRM results in the loss of some details, causing the garment patterns to become blurred in the third row. When the CSCM module is removed, the images in the first row exhibit issues such as coloring outside the edges and a loss of sketch stroke details. These problems become more pronounced when both modules are removed simultaneously, leading to noticeable unevenness in color distribution in some images. In contrast, replacing the LSTM module with the Transformer module yielded better visual effects than other situations, such as a gradient effect on the clothing in the first row. However, there are still challenges in retaining sketch details. These findings collectively confirm the effectiveness of each module in our model.

## VI. CONCLUSIONS

In this paper, we introduce HAI FIT, a creative sketch-to-image generation model tailored for fashion design. We effectively enhance both the global consistency of sketch feature vectors and the richness of intricate textures in the latent space through the proposed MFFN and CSCM. This enhancement enables the generation of high-quality, realistic clothing images. Furthermore, We present a fashion clothing dataset HAI Fashion for image translation to fill the gap in this field. We conduct extensive experiments comparing our method with state-of-the-art approaches. The qualitative and quantitative results robustly demonstrate the effectiveness of our proposed methodology in preserving sketch details and generating realistic images.

## REFERENCES

- [1] Youssef Alami Mejjati, Christian Richardt, James Tompkin, Darren Cosker, and Kwang In Kim. Unsupervised attention-guided image-to-image translation. *Advances in neural information processing systems*, 31, 2018.
- [2] Martin Arjovsky, Soumith Chintala, and Léon Bottou. Wasserstein generative adversarial networks. In *International conference on machine learning*, pages 214–223. PMLR, 2017.
- [3] Andrew Brock, Jeff Donahue, and Karen Simonyan. Large scale gan training for high fidelity natural image synthesis. *arXiv preprint arXiv:1809.11096*, 2018.
- [4] Tao Chen, Ming-Ming Cheng, Ping Tan, Ariel Shamir, and Shi-Min Hu. Sketch2photo: Internet image montage. *ACM transactions on graphics (TOG)*, 28(5):1–10, 2009.
- [5] Prafulla Dhariwal and Alexander Nichol. Diffusion models beat gans on image synthesis. *Advances in neural information processing systems*, 34:8780–8794, 2021.
- [6] Mathias Eitz, Ronald Richter, Kristian Hildebrand, Tamy Boubekeur, and Marc Alexa. Photosketcher: interactive sketch-based image synthesis. *IEEE Computer Graphics and Applications*, 31(6):56–66, 2011.
- [7] Ian Goodfellow, Jean Pouget-Abadie, Mehdi Mirza, Bing Xu, David Warde-Farley, Sherjil Ozair, Aaron Courville, and Yoshua Bengio. Generative adversarial nets. *Advances in Neural Information Processing Systems*, 27, 2014.
- [8] Kaiming He, Xiangyu Zhang, Shaoqing Ren, and Jian Sun. Deep residual learning for image recognition. In *Proceedings of the IEEE conference on computer vision and pattern recognition*, pages 770–778, 2016.
- [9] Martin Heusel, Hubert Ramsauer, Thomas Unterthiner, Bernhard Nessler, and Sepp Hochreiter. Gans trained by a two time-scale update rule converge to a local nash equilibrium. *Advances in neural information processing systems*, 30, 2017.

- [10] Jonathan Ho, Ajay Jain, and Pieter Abbeel. Denoising diffusion probabilistic models. *Advances in neural information processing systems*, 33:6840–6851, 2020.
- [11] Jonathan Ho and Tim Salimans. Classifier-free diffusion guidance. *arXiv preprint arXiv:2207.12598*, 2022.
- [12] Sepp Hochreiter and Jürgen Schmidhuber. Long short-term memory. *Neural computation*, 9(8):1735–1780, 1997.
- [13] Xun Huang, Ming-Yu Liu, Serge Belongie, and Jan Kautz. Multimodal unsupervised image-to-image translation. In *Proceedings of the European conference on computer vision (ECCV)*, pages 172–189, 2018.
- [14] Phillip Isola, Jun-Yan Zhu, Tinghui Zhou, and Alexei A Efros. Image-to-image translation with conditional adversarial networks. In *Proceedings of the IEEE conference on computer vision and pattern recognition*, pages 1125–1134, 2017.
- [15] Jianan Jiang, Di Wu, Zhilin Jiang, and Weiren Yu. Simple yet efficient: Towards self-supervised fg-sbir with unified sample feature alignment. *arXiv preprint arXiv:2406.11551*, 2024.
- [16] Tero Karras, Timo Aila, Samuli Laine, and Jaakko Lehtinen. Progressive growing of gans for improved quality, stability, and variation. *arXiv preprint arXiv:1710.10196*, 2017.
- [17] Tero Karras, Samuli Laine, and Timo Aila. A style-based generator architecture for generative adversarial networks. In *Proceedings of the IEEE/CVF conference on computer vision and pattern recognition*, pages 4401–4410, 2019.
- [18] Junho Kim, Minjae Kim, Hyeonwoo Kang, and Hee Kwang Lee. U-gat-it: Unsupervised generative attentional networks with adaptive layer-instance normalization for image-to-image translation. *ICLR*, 2020.
- [19] Alex Krizhevsky, Ilya Sutskever, and Geoffrey E Hinton. Imagenet classification with deep convolutional neural networks. *Advances in neural information processing systems*, 25, 2012.
- [20] Bo Li, Kaitao Xue, Bin Liu, and Yu-Kun Lai. Bdbm: Image-to-image translation with brownian bridge diffusion models. In *Proceedings of the IEEE/CVF Conference on Computer Vision and Pattern Recognition*, pages 1952–1961, 2023.
- [21] Runtao Liu, Qian Yu, and Stella X Yu. Unsupervised sketch to photo synthesis. In *Computer Vision—ECCV 2020: 16th European Conference, Glasgow, UK, August 23–28, 2020, Proceedings, Part III 16*, pages 36–52. Springer, 2020.
- [22] Ziwei Liu, Ping Luo, Shi Qiu, Xiaogang Wang, and Xiaoou Tang. Deepfashion: Powering robust clothes recognition and retrieval with rich annotations. In *Proceedings of IEEE Conference on Computer Vision and Pattern Recognition (CVPR)*, June 2016.
- [23] Mehdi Mirza and Simon Osindero. Conditional generative adversarial nets. *arXiv preprint arXiv:1411.1784*, 2014.
- [24] William Peebles and Saining Xie. Scalable diffusion models with transformers. In *Proceedings of the IEEE/CVF International Conference on Computer Vision*, pages 4195–4205, 2023.
- [25] Alec Radford, Luke Metz, and Soumith Chintala. Unsupervised representation learning with deep convolutional generative adversarial networks. *arXiv preprint arXiv:1511.06434*, 2015.
- [26] Robin Rombach, Andreas Blattmann, Dominik Lorenz, Patrick Esser, and Björn Ommer. High-resolution image synthesis with latent diffusion models. In *Proceedings of the IEEE/CVF conference on computer vision and pattern recognition*, pages 10684–10695, 2022.
- [27] Negar Rostamzadeh, Seyedarian Hosseini, Thomas Boquet, Wojciech Stokowiec, Ying Zhang, Christian Jauvin, and Chris Pal. Fashiongen: The generative fashion dataset and challenge. *arXiv preprint arXiv:1806.08317*, 2018.
- [28] Chitwan Saharia, William Chan, Huiwen Chang, Chris Lee, Jonathan Ho, Tim Salimans, David Fleet, and Mohammad Norouzi. Palette: Image-to-image diffusion models. In *ACM SIGGRAPH 2022 Conference Proceedings*, pages 1–10, 2022.
- [29] Karen Simonyan and Andrew Zisserman. Very deep convolutional networks for large-scale image recognition. *arXiv preprint arXiv:1409.1556*, 2014.
- [30] Jiaming Song, Chenlin Meng, and Stefano Ermon. Denoising diffusion implicit models. *arXiv preprint arXiv:2010.02502*, 2020.
- [31] Christian Szegedy, Wei Liu, Yangqing Jia, Pierre Sermanet, Scott Reed, Dragomir Anguelov, Dumitru Erhan, Vincent Vanhoucke, and Andrew Rabinovich. Going deeper with convolutions. In *Proceedings of the IEEE conference on computer vision and pattern recognition*, pages 1–9, 2015.
- [32] Ashish Vaswani, Noam Shazeer, Niki Parmar, Jakob Uszkoreit, Llion Jones, Aidan N Gomez, Łukasz Kaiser, and Illia Polosukhin. Attention is all you need. *Advances in neural information processing systems*, 30, 2017.
- [33] Ting-Chun Wang, Ming-Yu Liu, Jun-Yan Zhu, Andrew Tao, Jan Kautz, and Bryan Catanzaro. High-resolution image synthesis and semantic manipulation with conditional gans. In *Proceedings of the IEEE conference on computer vision and pattern recognition*, pages 8798–8807, 2018.
- [34] Zhou Wang, Alan C Bovik, Hamid R Sheikh, and Eero P Simoncelli. Image quality assessment: from error visibility to structural similarity. *IEEE transactions on image processing*, 13(4):600–612, 2004.
- [35] Di Wu, Zhiwang Yu, Nan Ma, Jianan Jiang, Yuetian Wang, Guixiang Zhou, Hanhui Deng, and Yi Li. Styleme: Towards intelligent fashion generation with designer style. In *Proceedings of the 2023 CHI Conference on Human Factors in Computing Systems*, pages 1–16, 2023.
- [36] Shaoan Xie, Mingming Gong, Yanwu Xu, and Kun Zhang. Unaligned image-to-image translation by learning to reweight. In *Proceedings of the IEEE/CVF International Conference on Computer Vision*, pages 14174–14184, 2021.
- [37] Han Zhang, Ian Goodfellow, Dimitris Metaxas, and Augustus Odena. Self-attention generative adversarial networks. In *International conference on machine learning*, pages 7354–7363. PMLR, 2019.
- [38] Richard Zhang, Phillip Isola, Alexei A Efros, Eli Shechtman, and Oliver Wang. The unreasonable effectiveness of deep features as a perceptual metric. In *Proceedings of the IEEE conference on computer vision and pattern recognition*, pages 586–595, 2018.
- [39] Jun-Yan Zhu, Taesung Park, Phillip Isola, and Alexei A Efros. Unpaired image-to-image translation using cycle-consistent adversarial networks. In *Proceedings of the IEEE international conference on computer vision*, pages 2223–2232, 2017.
- [40] Jun-Yan Zhu, Richard Zhang, Deepak Pathak, Trevor Darrell, Alexei A Efros, Oliver Wang, and Eli Shechtman. Toward multimodal image-to-image translation. *Advances in neural information processing systems*, 30, 2017.